IJE TRANSACTIONS B: Applications Vol. 34, No. 02, (February 2021) 536-546

International Journal of Engineering

Journal Homepage: www.ije.ir

Effects of Road Roughness, Aerodynamics, and Weather Conditions on Automotive Wheel Force

S. M. Saleh Mousavi-Bafrouyi[a], K. Reza Kashyzadeh*[b], S. M. Khorsandijou[a]

[a] *Department of Mechanical Engineering, South Tehran Branch, Islamic Azad University, Tehran, Iran*
[b] *Department of Mechanical and Instrumental Engineering, Academy of Engineering, Peoples' Friendship University of Russia (RUDN University), 6 Miklukho-Maklaya Street, Moscow, 117198, Russian Federation*

PAPER INFO

Paper history:
Received 09 October 2020
Received in revised form 31 October 2020
Accepted 06 November 2020

Keywords:
Aerodynamical Force
Air Temperature
Half-vehicle Model
Humidity
Road Roughness
Weather Conditions
Wheel Force

ABSTRACT

Taking road roughness, aerodynamics, and weather conditions, viz temperature and humidity, into consideration, the force applied to the wheel of a half-vehicle model traveling at constant speed has been calculated. A D-type rough horizontal road according to ISO 8606 evaluations was chosen for the experiment and the surface profile of which was measured by means of a topographic camera of Leica series to acquire discrete data to model the road roughness. The data have been converted from discrete points into smooth continuous linear functions with quadratic blends, because of the fact that the governing differential equations of motion of the vehicle model require the road roughness and the time rate of change of them. The line of action of wind or aero-dynamical force applied to vehicle model has been assumed to pass through the vehicle mass center. The vibrations of the half-vehicle model have been found via the Runge-Kutta method. Design of Experiments (DoE) has been used to investigate the effects of air temperature and humidity on the front and rear wheels. It was found that the value of force applied to the front wheel is far greater than that applied to the rear wheel (about 16.5%). Also, the role of the air temperature is much more effective on the wheel force than the air humidity. Moreover, the force of the front wheel is directly related to the values of weather parameters and the force of the rear wheel is inversely related to it.

***doi**: 10. 5829/ije.2021.34.02b.27*

Nomenclature

Ω	Spatial frequency	X_s	Vertical displacement of mass body
$Sg(\Omega)$	Power spectral density	X_{uf}	Vertical displacement of front tire
W	Total weight	X_{ur}	Vertical displacement of rear tire
W_f	Front wheel force	y_f	Applied external excitation to front wheel
W_r	Rear wheel force	y_r	Applied external excitation to rear wheel
α	Slope of road	K_{sf}	Front suspension stiffness
L	Distance between rear and front axles	K_{uf}	Front tire stiffness
b	Distance between front axle and gravity center	K_{sr}	Rear suspension stiffness
c	Distance between rear axle and gravity center	K_{ur}	Rear tire stiffness
h	Height of gravity center	C_{sf}	Front suspension damping
D_A	Aerodynamic force	C_{uf}	Front tire damping
h_a	Height position of aerodynamic loading	C_{sr}	Rear suspension damping
R_{hz}	Vertical load of tow	C_{ur}	Rear tire damping
R_{hx}	Longitudinal load of tow	L_f	Distance between front axle and center gravity
h_h	Height position of tow loading	L_r	Distance between rear axle and center gravity
d_h	Distance between location of tow loading and rear axle	V	Vehicle velocity

*Corresponding Author Institutional Email: *reza-kashi-zade-ka@rudn.ru* (K. Reza Kashyzadeh)

Please cite this article as: S. M. Saleh Mousavi-Bafrouyi, K. Reza Kashyzadeh, S. M. Khorsandijou, Effects of Road Roughness, Aerodynamics, and Weather Conditions on Automotive Wheel Force, International Journal of Engineering, B: Applications Vol. 34, No. 02, (2021) 536-546

F_{xf}	Thrust force of front wheel	C_d	Drag coefficient
F_{xr}	Thrust force of rear wheel	A	Reference area
R_{xf}	Rolling friction force between the front wheel and the ground	ρ	Air density
R_{xr}	Rolling friction force between the rear wheel and the ground	v	Flow velocity related to the vehicle
M_s	Body mass	P	Absolute pressure
I_s	Inertia moment of body	R	Specific gas constant
M_{uf}	Front tire mass	T	Temperature
M_{ur}	Rear tire mass	B	Barometric pressure
C	Center gravity of vehicle	P_v	Partial vapor pressure
θ	Rotation angle in the pitch motion	$\rho_{\%}$	Density of moist air

1. INTRODUCTION

Tire is a major connecting link between vehicle chassis and road surface, and transfers reaction force from road to the wheel of vehicle. It plays an important role in vehicle stability. The magnitude of the force applied to wheel of vehicle is dependent on vehicle velocity, road roughness, air flow or wind relative to vehicle surface, and weather conditions such as air temperature and humidity.

The road-tire contact force and the reaction force transmitted to vehicle wheel from road under snowy, rainy, and dry weather conditions has been investigated, and the effects of road roughness and weather parameters, namely air temperature, humidity and pressure, have been taken into consideration [1–3]. Influences of vehicle unbalanced-tires and air pressure, temperature and humidity over the dynamical behavior of vehicle have been investigated [4]. Stability and resonance of a one degree of freedom (DoF) quarter-car suspension model with hysteretic nonlinear dampers were studied by Naik and Singru [5]. Vibration of a nonlinear full-vehicle model was analyzed by Fakhraee et al. [6] for investigating the effect of passengers on the vibration. Kashyzadeh et al. [7] revealed the roles of road roughness type and vehicle speed in fatigue life of the steering knuckle, as a highly critical mechanical component of a vehicle. Ahmadi et al. [8] numerically estimated the fatigue life of the spot welds in the body of a vehicle vibrated due to passing over rough roads with various speeds.

Road roughness is referred to as the change of the height of road surface along and/or across the road (Figure 1). Several types of profilers such as topographic cameras are devices that are commonly used for measuring the profile of road roughness. For measuring road roughness, a few empirical procedures have been proposed by Sayers et al [9, 10]. Data collection of roughness of roads was accomplished by Sayers and Karamihas [11] for the Federal Highway Organization (FHO). González et al. [12] utilized accelerometers for estimating road roughness. Johannesson and Rychlik [13] applied time-invariant Laplace transform in order to model the features of road roughness in accordance with ISO and IRI standards.

Vehicle dynamics has been simulated by Imine et al. [14] who took road roughness profile and road-tires contact force into consideration. Vehicle passive and semi-active suspension systems have been analyzed under the influence of road roughness by Reza Kashyzadeh et al. [15]. Samandari and Rezaee [16] have investigated the influence of road roughness over the dynamical behavior of quarter and half-vehicle models with nonlinear springs and dampers.

Performance of suspension system was optimized by Shojaeefard et al. [17] via multi-objective theory and the optimum stiffness for spring and the optimum coefficient for damper were found for driver seat of a five DoF vehicle model passing over a rough road with random profile. Recently, various data mining techniques and DOE algorithms have been highly regarded by automotive engineers in order to optimize and improve product quality. Naga Raju et al. [18] have used Taguchi design algorithm-based on the finite element simulation to assess the static behavior of leaf spring with the aim of choosing the most suitable material for its manufacture. Also, the grey-fuzzy-Taguchi method has been used to optimize the beam-like structure of a vehicle body [19]. Zhang and Wang [20] have investigated and optimized the suspension system of the half-vehicle model integrated with an arm-teeth regenerative shock absorber by utilizing Taguchi approach.

Based on the literature review, many researchers have studied the effects of road conditions on the dynamic behavior of auto parts. However, other influential parameters such as weather conditions (i.e., air temperature, humidity, wind speed and wind direction)

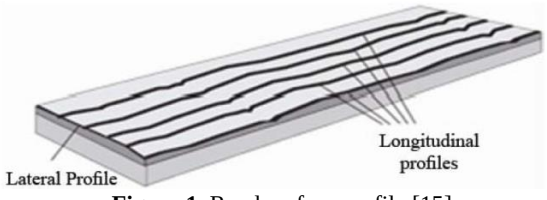

Figure 1. Road surface profile [15]

have been rarely considered (there is only qualitative expression for them). Therefore, one of the novelty of the present research is to investigate the effects of different parameters simultaneously on the vehicle wheel forces. In this regard, the rear- and front-wheel force were calculated based on the parameters variations including road roughness (laboratory data using topographic camera), aerodynamics, and weather factors. Also, it was done by assuming constant vehicle velocity and neglecting slope of road, dive acceleration, and load of tow. Next, the Runge-Kutta (RK) method was used to solve the vibration equations of half-car model. Eventually, for the first time, Taguchi approach (TA) as one of the well-known DOE techniques was applied to analyze the sensitivity of the wheel forces to parameter changes. The most important and ineffective parameters on the front and rear wheel forces were reported.

2. ROAD ROUGHNESS MEASUREMENT

Different methods have been presented to evaluate road roughness. Among all of them, there are two common and practical methods. The First method uses a topographic camera that directly records ups and downs of the road (geometrical measurement). In other words, road roughness are measured using static devices such as topographic camera. Figure 2 presents a schematic of the implementation of this process [9]. Another method is response type approaches which work on the basis of data collected from different types of sensors installed in different parts of the car [21–23]. Therefore, these methods are called dynamic data collection. It means that the equipment is installed on the car body or axle and data is taken while the car is moving. These equipments include laser profilometer, mobile measuring devices, accelerometers, h-sensor, and vibrometer. After data collection, a calibrated relationship can be extracted using a programming code (MATLAB) and road classification standards based on the Power Spectral Density (PSD) function.

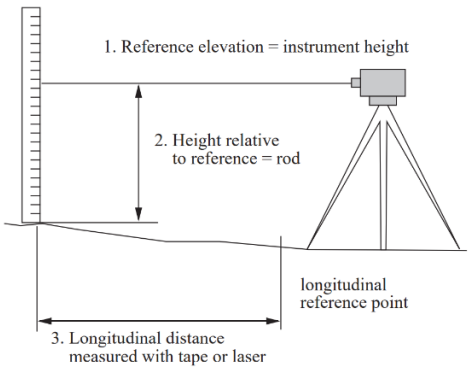

Figure 2. Schematic of topographic camera performace for measuring road profile [9]

In the present research, road data collection was performed using topographic camera of Leica series of total Station TS02 model (Figure 3). In this camera model, angular and longitudinal accuracy are 7 second and 2 picometer, respectively.

The mapping was conducted on an asphalt suburban road by recording 500 points. Next, numerical integration method, i.e., Simpson's rule was used to calculate Power Spectral Density (PSD) function. Figure 4 depicts the PSD of asphalt suburban road based on the mapping data.

The mentioned road was considered as D-class compared to the road classification of ISO-8606 [24]. According to this standard, as illustrated in Figure 5, the road roughness approximates by two straight lines and different slopes in the log-log scale.

The PSD in terms of spatial frequency (1/wavelength) is calculated from the following formula [24]:

$$if \quad \Omega \le \frac{1}{2\pi} \quad then \quad S_g(\Omega) = S_g(\Omega_0) \times \left(\frac{\Omega}{\Omega_0}\right)^{-N_1} \tag{1}$$

$$if \quad \Omega > \frac{1}{2\pi} \quad then \quad S_g(\Omega) = S_g(\Omega_0) \times \left(\frac{\Omega}{\Omega_0}\right)^{-N_2} \tag{2}$$

Figure 3. Topographic camera of leica series of total station TS02 model

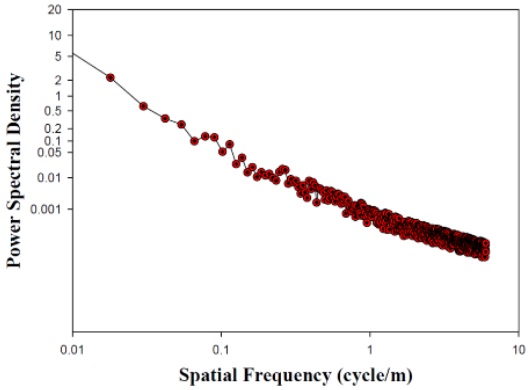

Figure 4. PSD of asphalt suburban road based on the mapping data in the present research

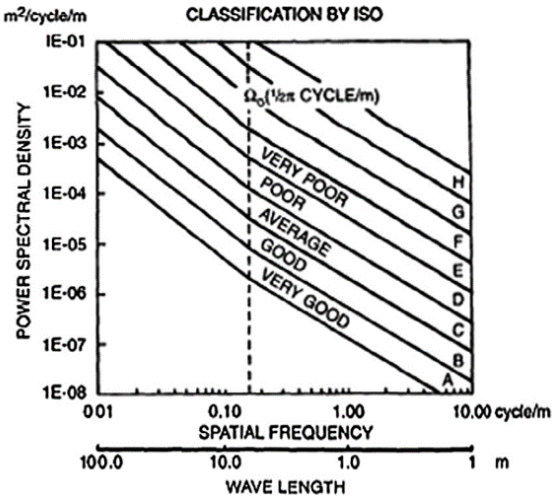

Figure 5. Proposed road roughness classification by ISO (International Standard Organization) [24]

Table 1 presents the value of $S_g(\Omega_0)$ considering the spatial frequency of $\Omega_0 = \frac{1}{2\pi}\ Cycle/m$ for different roads [25]. Also, constant coefficients of N_1 and N_2 are 2.0 and 1.5, respectively.

Obviously, the road profile is constant, nevertheless, the tires cannot touch all the roughness. In other words, there is a difference between real road roughness and its simulation as the external excitation. Moreover, the jump phenomenon occurs at high vehicle speeds. Therefore, the vehicle, especially wheels and tires, does not experience some parts of road roughness. However, in some cases, these jumps can be considered as new elevation with larger amplitude. In the previous researches, the second author of the current paper has studied the effect of vehicle velocity on the simulation of road roughness [26]. The results showed that low and high speeds had a negligible effect on high quality road (e.g., road class A). Furthermore, these effects will be visible on the bad quality road like road class E.

In the present research, the vehicle velocity of 80 km/h was considered to evaluate excitation. Selection of this speed may be justified; as it is allowable driving speed on suburban roads of different Asian countries. Figure 6 illustrates the time history of this excitation.

TABLE 1. Parametrical classification of road roughness suggested by ISO [24, 25]

Road Class	Degree of Roughness Range	$S_g(\Omega_0)\cdot 10^{-6}\ m^2/cycles/m$ Geometric Mean
A (Very Good)	< 8	4
B (Good)	8 – 32	16
C (Average)	32 – 128	64
D (Poor)	128 – 512	256
E (Very Poor)	512 – 2048	1024
F	2048 – 8192	2048
G	8192 – 32768	4096
H	More than 32768	16384

3. VERTICAL VIBRATION OF THE HALF-CAR MODEL

Figure 7 illustrates a half-car model with four Degrees of Freedom (DoF). The Lagrange's method was used to derive vibration equations (Equation (3)).

$$[M][\ddot{S}]+[C][\dot{S}]+[K][S]=[F] \quad (3)$$

where

$$[K]=\begin{bmatrix} K_{sr}+K_{sf} & -K_{sf} & -K_{sr} & K_{sf}L_f-K_{sr}L_r \\ -K_{sf} & K_{sf}+K_{uf} & 0 & -K_{sf}L_f \\ -K_{sr} & 0 & K_{sr}+K_{ur} & K_{sr}L_r \\ K_{sf}L_f-K_{sr}L_r & -K_{sf}L_f & K_{sr}L_r & K_{sr}L_r^{\,2}+K_{sf}L_f^{\,2} \end{bmatrix} \quad (4)$$

$$[C]=\begin{bmatrix} C_{sr}+C_{sf} & -C_{sf} & -C_{sr} & C_{sf}L_f-C_{sr}L_r \\ -C_{sf} & C_{sf}+C_{uf} & 0 & -C_{sf}L_f \\ -C_{sr} & 0 & C_{sr}+C_{ur} & C_{sr}L_r \\ C_{sf}L_f-C_{sr}L_r & -C_{sf}L_f & C_{sr}L_r & C_{sr}L_r^{\,2}+C_{sf}L_f^{\,2} \end{bmatrix} \quad (5)$$

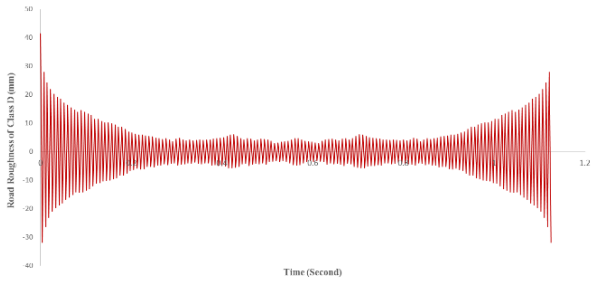

Figure 6. Time-history of excitation for an asphalt suburban road (Class D)-vehicle velocity of 80 km/h

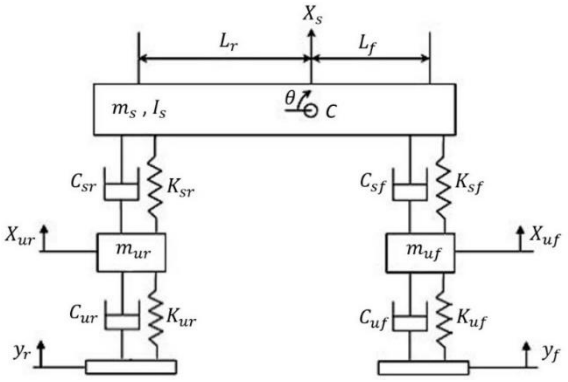

Figure 7. The 4-DoF half-car model (bicycle model) considering two separated external excitations [27]

$$[M]=diag(M_s, M_f, M_r, I_s)=\begin{bmatrix} M_s & 0 & 0 & 0 \\ 0 & M_f & 0 & 0 \\ 0 & 0 & M_r & 0 \\ 0 & 0 & 0 & I_s \end{bmatrix} \quad (6)$$

$$[F]=\begin{bmatrix} 0 & 0 \\ 0 & C_{uf} \\ C_{ur} & 0 \\ 0 & 0 \end{bmatrix}\begin{bmatrix} \dot{Y}_r \\ \dot{Y}_f \end{bmatrix}+\begin{bmatrix} 0 & 0 \\ 0 & K_{uf} \\ K_{ur} & 0 \\ 0 & 0 \end{bmatrix}\begin{bmatrix} Y_r \\ Y_f \end{bmatrix} \quad (7)$$

The elements of the above matrices, viz $[M],[C],[K],[S],[F],[\dot{S}],[\ddot{S}],Y_r,Y_f,M_s,M_f,M_r,I_s,L_f,L_r,K_{sr},K_{sf},K_{uf},K_{ur},C_{sr},C_{sf},C_{uf}$ and C_{ur} are introduced in Nomenclature.

The body and suspension system containing tire were considered as sprung and un-sprung masses, respectively. The Runge-Kutta (RK) method was used to solve coupled equations of vibration.

The motion Equation (3) and the excitation forces (7) show that a travelling half-car model is excited by the roughness and the time rate of change of them. The speed of the travelling half-car model is assumed 80 km/h in this article. Time rate of change of the road roughness can appropriately be achieved neither from discretely-acquired road roughness nor from non-smooth reconstruction of the road roughness. As a result, a smooth reconstruction of the road roughness is required, because, contrary to non-smooth curves and discrete data, smooth curves are differentiable. In this regard, a smooth curve including linear functions with quadratic blends has been proposed in Appendix A for smooth reconstruction of the road roughness from discretely-acquired data [28].

The governing differential equations of motion of the vehicle model requires road roughness and the time rate of change of the roughness as excitation. The excitations to the rear and front wheels have been considered the same, but with a delay time. The delay time depends on the vehicle velocity and the distance between the two axles, and is calculated using the following equation.

$$time\ delay:\quad t=\frac{L}{speed}=\frac{2415\ mm}{80\ km/hr}=0.108675\ s \quad (8)$$

The road roughness are available in discrete form from experiment, but the smooth continuous form of them are required by the vehicle governing equations as well as the continuous time-rate of change of them. As a smooth continuous form of the road roughness, the linear functions with quadratic blends according to Appendix A and Figure 8 has been taken into consideration. The reconstruction by linear functions smoothly connected by quadratic functions are plotted in black color in Figure 8 where a non-smooth continuous reconstruction of road roughness by linear functions is plotted in red.

Expressions (A1)-(A7) of Appendix A show how one might construct a smooth countinuous function for road roughness, namely a smooth function composed of adequate linear functions being smoothly connected to each other. Obviously, the rate of change of the smooth function is a non-smooth continuous function.

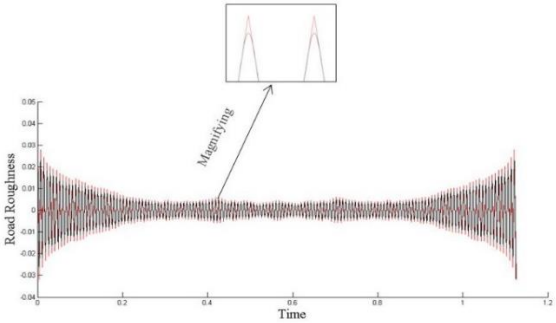

Figure 8. Smooth reconstruction of road roughness by linear functions with quadratic blends (plotted in black) according to Apendix A, and non-smooth reconstruction of road roughness by linear functions (plotted in red) from discretely-acquired road roughness (time axis in seconds represents the axis of distance divided by the vehicle velocity of 80 km/h).

Eventually, the height fluctuation of gravity center was extracted. The values of parameters used in this research based on an Iranian passenger car are reported in Table 2 [29].

4. WHEEL FORCE CALCULATION IN TERMS OF WEATHER PARAMETERS

Dynamic equations were derived for a full vehicle on steep road. A schematic of these forces and their location is shown in Figure 9.

TABLE 2. Vehicle parameters [29]

Symbol	Value	Unit
m_s	1347	kg
I_s	2160	Kg. m
m_{uf}	42.218	kg
m_{ur}	42.218	kg
K_{sf}	35900	N/m
K_{uf}	173000	N/m
K_{sr}	33100	N/m
K_{ur}	173000	N/m
C_{sf}	1368	Ns/m
C_{uf}	3105	Ns/m
C_{sr}	1368	Ns/m
C_{ur}	3105	Ns/m
L_f	1.090624	m
L_r	1.324376	m

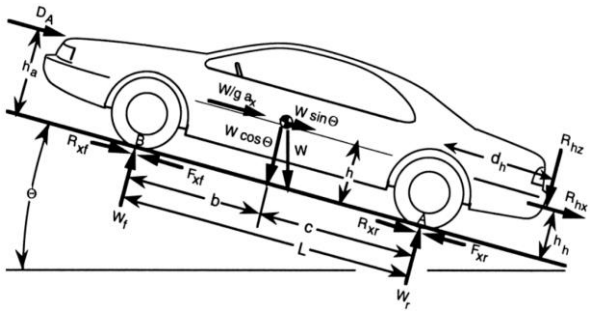

Figure 9. Vehicle dynamics analysis on the steep road [27]

The wheel forces were achieved by using torque calculation at point A and B locating under the rear- and front-tires, respectively (Equation (9) and Equation (10)). Clearly, the sum of torques at point A is zero by neglecting dive acceleration [27].

$$W_f = \frac{-1}{L}\left[D_A\, h_A + \frac{W}{g} a_x\, h + R_{hx}\, h_h + R_{hz}\, d_h + W h \sin(\alpha) + W c \cos(\alpha)\right] \quad (9)$$

$$W_r = \frac{1}{L}\left[D_A\, h_A + \frac{W}{g} a_x\, h + R_{hx}\, h_h + R_{hz}\,(d_h + L) + W h \sin(\alpha) + W b \cos(\alpha)\right] \quad (10)$$

In the present research, the wheel forces were calculated by assuming constant vehicle velocity of 80 km/h and neglecting slope of road, dive acceleration, and load of tow. The drag, in the vehicle aerodynamic is calculated using Equation (11):

$$D_A = \frac{C_d A \rho v^2}{2} \quad (11)$$

Air density is a function of temperature, pressure, and humidity. The air density is about 1.225 kg/m^3 at the sea level and temperature of 15 °C [30]. Figure 10 shows air density vs temperature.

In addition to the above-mentioned conditions, the density of air will vary as humidity content. The water vapor is a relatively light gas compared to diatomic oxygen and nitrogen. Therefore, when water vapor increases, the amount of oxygen and nitrogen decrease per unit volume, and then the density decreases because the mass is decreasing [31]. Figure 11 shows the air density vs humidity. Also, the empirical relation between density and humidity is defined by Equation (12) [31]:

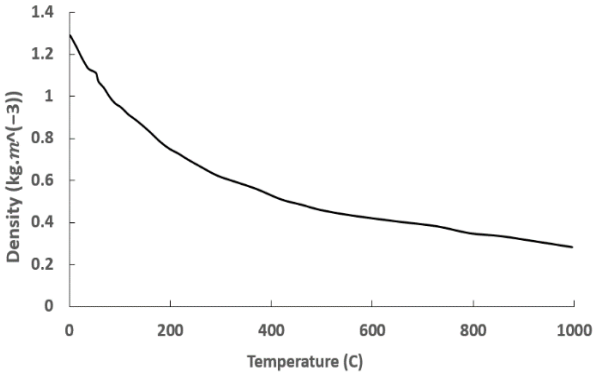

Figure 10. Air density versus temperature [30]

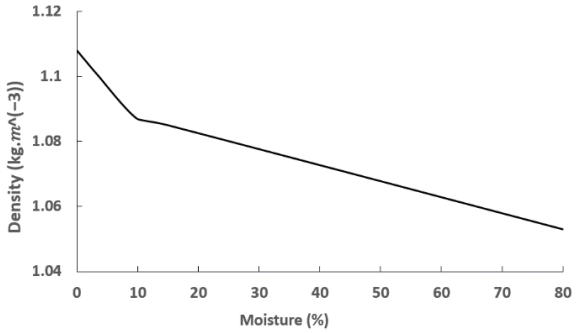

Figure 11. Air density versus humidity [31]

$$\rho_{\%} = 1.2929 \times \frac{273.15}{T} \times \frac{B - 0.3783\, P_v}{1.013 \times 10^5} \quad (12)$$

where T is temperature in Kelvin, B and P_v are barometric pressure and partial vapor pressure in Pascal, respectively.

To study the effect of wind on the wheel forces, time history of wind speed was used based on meteorological data [32]. The wind loading versus time for stormy weather is demonstrated in Figure 12. Moreover, three different wind directions ($\theta = 0°. 90°.\ and\ 180°$) were considered to evaluate wind effect on the wheel forces. Therefore, zero value of θ means the direction of the wind and the movement of the car are the same.

5. DESIGN OF EXPERIMENT

To study the effects of weather parameters on the wheel forces of passenger car, Taguchi Approach (TA) as one of the well-known Design of Experiment (DOE) techniques was used [33–35]. To this end, four parameters, including wind speed, wind direction, air temperature, and air humidity were considered as input variables. Also, the maximum values of rear- and front-wheel forces were considered as output parameters. Different levels of input parameters used in this research are presented in Table 3.

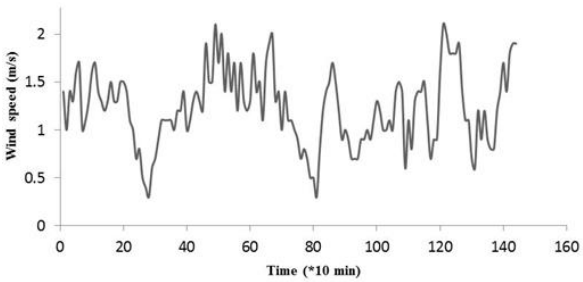

Figure 12. Wind loading versus time for stormy weather [32]

TABLE 3. Variables and their levels used as input data in the present research

Parameters	Symbol	Levels		
		L1	L2	L3
Wind speed (m/s)	V	1	1.2	1.4
Wind direction ($degree$)	θ	0	90	180
Air temperature (℃)	T	0	20	40
Air humidity (%)	M	0	40	80

To perform Taguchi sensitivity analysis, the formulation of smaller is better was considered for both rear- and front-wheel forces. The L9 orthogonal matrix was used as reported in Table 4.

6. RESULTS AND DISCUSSION

The wheel forces variation depends on temperature and humidity are demonstrated in Figures 13 and 14, respectively. As Figure 13-a clearly shows, the front-wheel force increases by increasing air temperature. However, this change is not significant (e.g., raising the temperature from zero to 60 degrees will only lead to a change in front-wheel force about 0.1 %). But, the rear-wheel force decreases by increasing air temperature (Figure 13-b). Also, the effect of temperature changes on the rear-wheel force is greater than its effect on the front-wheel force (the reduction in the rear-wheel force is approximately 0.15 % by increasing the air temperature from zero to 60 degrees). Moreover, it is clear that the value of force on the front wheel is far greater than the force on the rear wheel. In the case of T=20 ℃, the force difference between the rear and front wheels is about 16.5 %.

From Figure 14, as the air humidity increases, the value of force on the front and rear wheels increases and decreases, respectively, but these changes are negligible.

TABLE 4. The Orthogonal Matrix of Taguchi for L9

Run No.	V	θ	T	M
1	L1	L1	L1	L1
2	L1	L2	L2	L2
3	L1	L3	L3	L3
4	L2	L1	L2	L3
5	L2	L2	L3	L1
6	L2	L3	L1	L2
7	L3	L1	L3	L2
8	L3	L2	L1	L3
9	L3	L3	L2	L1

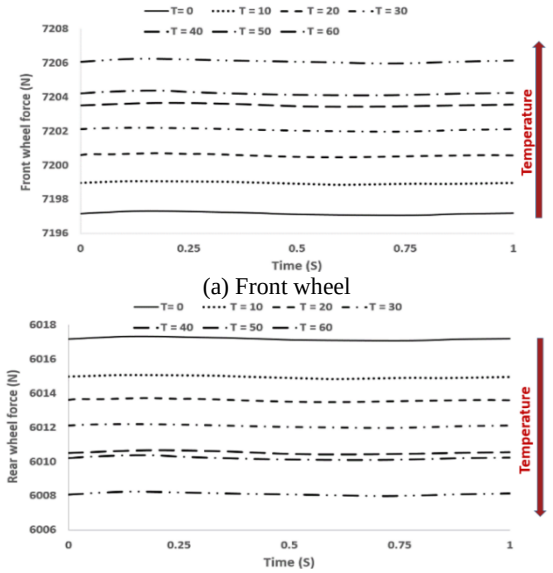

(a) Front wheel

(b) Rear wheel

Figure 13. Effect of air temperature (in celsius) on wheels force

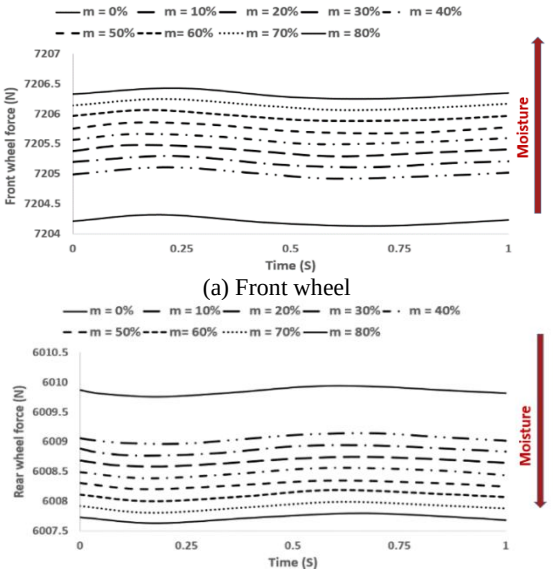

(a) Front wheel

(b) Rear wheel

Figure 14. Effect of air humidity (in percentage) on wheels force

The force changes for both wheels are the same (maximum of 0.03 %).

Next, Figure 15 shows the effect of wind direction on the wheel forces. The value of front-wheel force is maximum when the direction of the wind and the movement of the vehicle are opposite. And in this case, the value of the rear-wheel force is minimal. The results show that the maximum change in force due to the wind direction in the front and rear wheels is approximately 0.14 and 0.17 %, respectively.

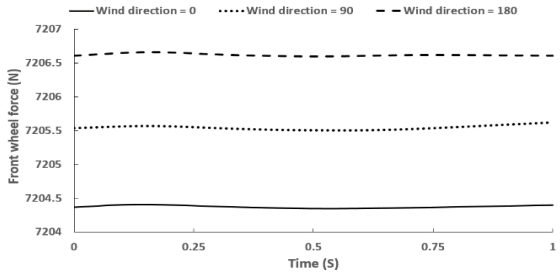

(a) Front wheel

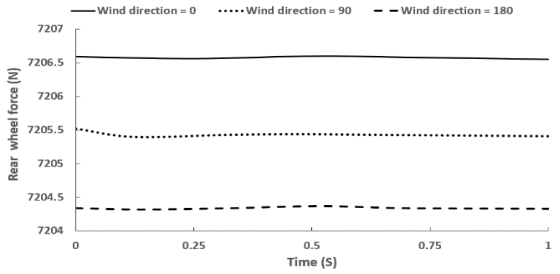

(b) Rear wheel

Figure 15. Effect of wind direction (in degrees) on wheels force

In Taguchi approach, the main effect plots for means and signal to noise ratios were used to compare the wheel force effects against other factors. Figures 16 and 17 show these diagrams for front- and rear-wheel, respectively.

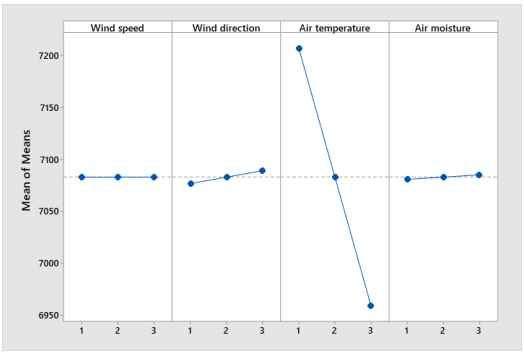

(a) Mean of means

(b) Mean of SN ratios

Figure 16. Means of front wheel force under the influence of wind, temperature, and humidity

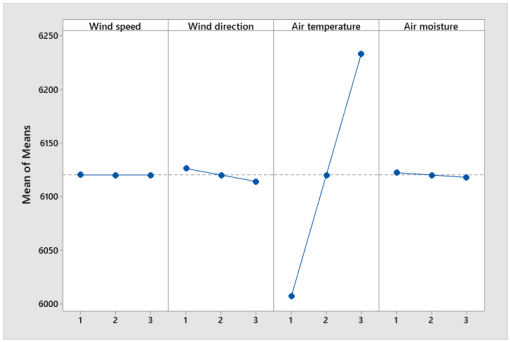

(a) Mean of means

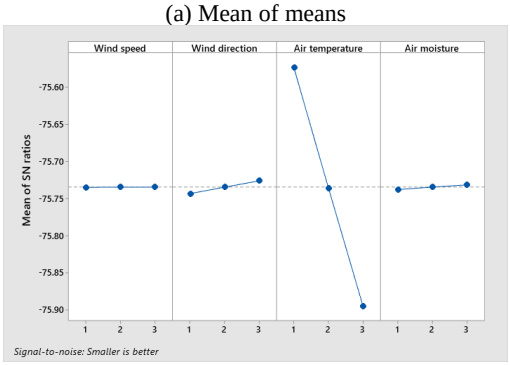

(b) Mean of SN ratios

Figure 17. Means of rear wheel force under the influence of wind, temperature, and humidity

The above-diagrams show that the number of data for parameters wind direction, air temperature, and air humidity is acceptable. But, the results show that the wind speed parameter cannot be discussed. Because, the number of data for this parameter is insufficient or the value range considered for this parameter has no effect on the wheel force. In other words, changes in wind speed on a stormy day are ineffective. Therefore, it is recommended, in future research, to study the effects of wind speed in a stormy day relative to a calm day. Based on the results obtained by Taguchi approach, the wheel force is mainly affected by air temperature (Figure 18). Moreover, the results indicate that air humidity is the most ineffective parameter on the value of force in both front and rear wheels.

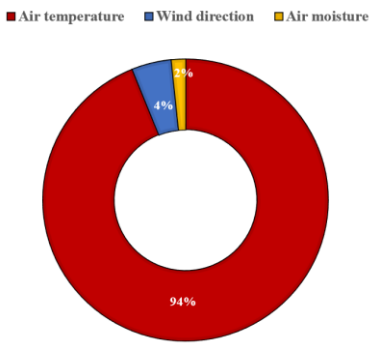

(a) Front wheel force

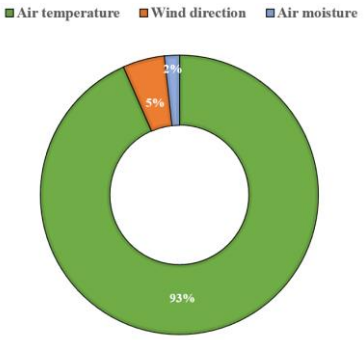

(b) Rear wheel force

Figure 18. Roles of air humidity and wind direction vis-à-vis that of air temperature in wheels forces found based on taguchi sensitivity analysis

7. CONCLUSION

In this study, the wheel forces of a passenger car were calculated in terms of weather parameters. Firstly, road roughness was measured using a topographic camera, then the classification of desired road was determined by utilizing Fast Fourier Transform (FFT) function and comparison with the ISO standard. Road class-D and vehicle velocity of 80 Km/h were considered as external excitation for both front and rear wheels with a delay time. The RK method was used to solve the coupled vibration equations of half-car model, and the height fluctuation of gravity center was extracted. Eventually, dynamic equations were introduced to calculate wheel force in terms of weather parameters. Next, the effects of various parameters (wind speed, wind direction, air temperature, and air humidity) were investigated on the wheel forces using numerical analysis and Taguchi sensitivity analysis. The most important achievements of this research are:

- The value of force applied to the front wheel is far greater than that applied to the rear wheel. The difference between the forces is about 16.5 % at T = 20 ℃.
- By increasing the air temperature, the front wheel force increases and the rear wheel force decreases. The amount of decrease in the rear wheel force is greater than the amount of increase in the front wheel force.
- By increasing the air humidity, the front wheel force very slightly increases and the rear wheel force very slightly decreases.
- The results found through Taguchi approach reveal that the air temperature is the most effective parameter and the air humidity is the least effective parameter with respect to the parameters investigated in this research.
- The results of this research indicate that variations of wind speed on a stormy day have no effect on the wheel forces.

8. ACKNOWLEDGMENTS

This paper has been supported by the RUDN University Strategic Academic Leadership Program.

9. REFERENCES

1. Waluś, K. J., and Olszewski, Z., "Analysis of Tire-road Contact Under Winter Conditions", Proceedings of the World Congress on Engineering 2011 Vol III, London, U.K., (2011), 1–4.
2. Ghandour, R., Victorino, A., Doumiati, M., and Charara, A., "Tire/road friction coefficient estimation applied to road safety", 18th Mediterranean Conference on Control and Automation, MED'10, (2010), 1485–1490. doi:10.1109/MED.2010.5547840
3. Ahn, C. S., Robust Estimation of Road Friction Coefficient for Vehicle Active Safety Systems, PhD dissertation, University of Michigan.
4. Sayers, M. W., Gillespie, T. D., Paterson, W. D. 0, World, T., and Washington, B., Guidelines for Conducting and Calibrating Road Roughness Measurements,University of Michigan, Ann Arbor, Transportation Research Institute, (1986).
5. Naik, R. D., and Singru, P. M., "Resonance, stability and chaotic vibration of a quarter-car vehicle model with time-delay feedback", ***Communications in Nonlinear Science and Numerical Simulation***, Vol. 16, No. 8, (2011), 3397–3410. doi:10.1016/j.cnsns.2010.11.006
6. Fakhraee, J., Mohammad Khanlo, H., Ghayour, M., & Faramarzi, K. (2016). The influence of road bumps characteristics on the chaotic vibration of a nonlinear full-vehicle model with driver. **International Journal of Bifurcation and Chaos**, 26(9), 1650151. DOI: 10.1142/S0218127416501510
7. Reza Kashyzadeh, K., Farrahi, G. H., Shariyat, M., and Ahmadian, M. T., "Experimental accuracy assessment of various high-cycle fatigue criteria for a critical component with a complicated geometry and multi-input random non-proportional 3D stress components", ***Engineering Failure Analysis***, Vol. 90, (2018), 534–553. doi:10.1016/j.engfailanal.2018.03.033
8. Ahmadi, A., Farrahi, G. H., Kashyzadeh, K. R., Azadi, S., and Jahani, K., "A comparative study on the fatigue life of the vehicle body spot welds using different numerical techniques: Inertia relief and modal dynamic analyses", ***Frattura Ed Integrita Strutturale***, Vol. 14, No. 52, (2020), 67–81. doi:10.3221/IGF-ESIS.52.06
9. Sayers, M. W., and Karamihas, S. M., The Little Book of Profiling Basic Information about Measuring and Interpreting Road Profiles, University of Michigan, Ann Arbor, Transportation Research Institute, (1998).
10. Sayers, M. W., Gillespie, T. D., and V Queiroz, C. A., The International Road Roughness Experiment Establishing Correlation and a Calibration Standard for Measurements, University of Michigan, Ann Arbor, Transportation Research Institute, (1986).
11. Sayers, M. W., and Karamihas, S. M., interpretation of road roughness profile data, University of Michigan Transportation Research Institute, (1996).
12. González, A., O'Brien, E. J., Li, Y. Y., and Cashell, K., "The use of vehicle acceleration measurements to estimate road roughness", ***Vehicle System Dynamics***, Vol. 46, No. 6, (2008), 483–499. doi:10.1080/00423110701485050
13. Johannesson, P., and Rychlik, I., "Modelling of road profiles using roughness indicators", ***International Journal of Vehicle Design***, Vol. 66, No. 4, (2014), 317–346. doi:10.1504/IJVD.2014.066068

14. Imine, H., Delanne, Y., and M'Sirdi, N. K., "Road profile input estimation in vehicle dynamics simulation", ***Vehicle System Dynamics***, Vol. 44, No. 4, (2006), 285–303. doi:10.1080/00423110500333840
15. Reza-Kashyzadeh, K., Ostad-Ahmad-Ghorabi, M. J., and Arghavan, A., "Investigating the effect of road roughness on automotive component", ***Engineering Failure Analysis***, Vol. 41, (2014), 96–107. doi:10.1016/j.engfailanal.2013.12.008
16. Samandari, H., and Rezaee, M., "The stability and chaos analysis of a nonlinear wheeled vehicle model under road excitation", ASME 2010 10th Biennial Conference on Engineering Systems Design and Analysis, ESDA2010, Vol. 3, (2010), 115–120. doi:10.1115/ESDA2010-24451
17. Shojaeefard, M. H., Khalkhali, A., and Erfani, P. S., "Multi-Objective Suspension Optimization of a 5-DOF Vehicle Vibration Model Excited by Random Road Profile", ***International Journal of Advanced Design and Manufacturing Technology***, Vol. 7, No. 1, (2014), 1–7.
18. Raju, B. N., Kranthi Kiran, G., Manojana, P., Sateesh, K., Yashaswini, K., and Babu, K., "Material Selection and STATIC Analysis of Leaf spring Using FEA and Taguchi Method", ***JAC : A Journal of Composition Theory***, Vol. 13, No. 3, (2020), 497–509
19. Yao, W., Cai, K., and Xu, Y., "Optimizing the beam-like structure of a vehicle body using the grey–fuzzy–Taguchi method", ***Engineering Optimization***, Vol. 53, No. 1, (2021), 49–70. doi:10.1080/0305215X.2019.1698033
20. Zhang, R., and Wang, X., "Parameter study and optimization of a half-vehicle suspension system model integrated with an arm-teeth regenerative shock absorber using Taguchi method", ***Mechanical Systems and Signal Processing***, Vol. 126, (2019), 65–81. doi:10.1016/j.ymssp.2019.02.020
21. Mahmoudzadeh, A., Golroo, A., Jahanshahi, M., and Firoozi Yeganeh, S., "Estimating Pavement Roughness by Fusing Color and Depth Data Obtained from an Inexpensive RGB-D Sensor", ***Sensors***, Vol. 19, No. 7, (2019), 1655. doi:10.3390/s19071655
22. Abulizi, N., Kawamura, A., Tomiyama, K., and Fujita, S., "Measuring and evaluating of road roughness conditions with a compact road profiler and ArcGIS", ***Journal of Traffic and Transportation Engineering (English Edition)***, Vol. 3, No. 5, (2016), 398–411. doi:10.1016/j.jtte.2016.09.004
23. Arbabpour Bidgoli, M., Golroo, A., Sheikhzadeh Nadjar, H., Ghelmani Rashidabad, A., and Ganji, M. R., "Road roughness measurement using a cost-effective sensor-based monitoring system", ***Automation in Construction***, Vol. 104, (2019), 140–152. doi:10.1016/j.autcon.2019.04.007
24. Wong, J., Theory of Ground Vehicles, (2008) John Wiley & Sons.
25. Nickmehr, N., Ride Quality and Drivability of a Typical Passenger Car subject to Engine/Driveline and Road Non-uniformities Excitations, Master thesis, Linkoping University of Sweden, (2011).
26. Reza-Kashyzadeh, K., Ostad-Ahmad-Ghorabi, M. J., and Arghavan, A., "Study effects of vehicle velocity on a road surface roughness simulation", ***Applied Mechanics and Materials***, Vol. 372, (2013), 650–656. [In Persian] doi:10.4028/www.scientific.net/AMM.372.650
27. Gillespie, T., Fundamentals of Vehicle Dynamics, (Vol. 400). Warrendale, PA: Society of Automotive Engineers, (1992).
28. Craig, J. J., Introduction to Robotics, Pearson Education International, (2005).
29. Reza Kashyzadeh, K., Farrahi, G. H., Shariyat. M., & Ahmadian. M. T. (2018). The role of wheel alignment over the fatigue damage accumulation in vehicle steering knuckle. **Journal of Stress Analysis,** 3(1), 21-33. DOI: 10.22084/jrstan.2018.15722.1042
30. ICAO, Manual of the ICAO Standard Atmosphere, Doc 7488-CD, Third Edition, (1993), ISBN 92-9194-004-6.
31. Monteith, J., and Unsworth, M., "Principles of environmental physics", (2008).
32. Reza Kashyzadeh, K. (2015). Fatigue life estimation under multi-axial random loading in light poles. **Ciência e Natura**, 37(6-1), 183-189. DOI: 10.5902/2179460X20845
33. Farrahi, G. H., Reza Kashyzadeh, K., Minaei, M., Sharifpour, A., and Riazi, S., "Analysis of resistance spot welding process parameters effect on the weld quality of three-steel sheets used in automotive industry: Experimental and finite element simulation", ***International Journal of Engineering, Transactions A: Basics***, Vol. 33, No. 1, (2020), 148–157. doi:10.5829/ije.2020.33.01a.17
34. Maleki, E., Unal, O., and Reza Kashyzadeh, K., "Efficiency Analysis of Shot Peening Parameters on Variations of Hardness, Grain Size and Residual Stress via Taguchi Approach", ***Metals and Materials International***, Vol. 25, No. 6, (2019), 1436–1447. doi:10.1007/s12540-019-00290-7
35. Omidi Bidgoli, M., Reza Kashyzadeh, K., Rahimian Koloor, S. S., and Petru, M., "Estimation of Critical Dimensions for the Crack and Pitting Corrosion Defects in the Oil Storage Tank Using Finite Element Method and Taguchi Approach", ***Metals***, Vol. 10, No. 10, (2020), 1372. doi:10.3390/met10101372

APPENDIX A

Smoothly-reconstructing Road Roughness from Discretely-acquired Road Roughness by Linear Functions with Quadratic Blends

The discretely-acquired data of the road roughness y_n at t_n are given by (A1).

$$\begin{aligned} & t_1 < t_2 < \cdots < t_{n-1} < t_n < t_{n+1} < \cdots < t_{N-1} < t_N \\ & y_n \equiv y(t_n) \qquad , \quad 1 \le n \le N \end{aligned} \tag{A1}$$

Considering the parameters in (A2), and in order to smoothly-reconstruct the road roughness, a smooth curve might be composed of the connection lines (A3) between each couple of adjacent points of the discretely-acquired data of the road roughness (A1) and the quadratic blends (A4) between them.

$$\begin{aligned} & t_1 = \beta_1 < \cdots < \beta_{n-2} < \alpha_{n-1} < t_{n-1} < \beta_{n-1} < \alpha_n < t_n < \beta_n < \alpha_{n+1} < t_{n+1} < \beta_{n+1} < \cdots < \beta_{N-1} < \alpha_N = t_N \\ & \beta_{n-1} < \alpha_n < t_n < \beta_n \qquad , \quad 2 \le n \le N-1 \end{aligned} \tag{A2}$$

$$\begin{cases} y(t)=m_n t+h_n \quad , \quad \beta_{n-1}\le t\le \alpha_n \quad , \quad 2\le n\le N \\ \dot{y}(t)=m_n \\ \ddot{y}(t)=0 \end{cases} \qquad \begin{cases} m_n \equiv \dfrac{y_n-y_{n-1}}{t_n-t_{n-1}} \\ h_n \equiv y_n - m_n t_n \end{cases} \tag{A3}$$

$$\begin{cases} y(t)=a_n t^2+b_n t+c_n \quad , \quad \alpha_n < t < \beta_n=\alpha_n+\tau_n \quad , \quad 2\le n\le N-1 \\ \dot{y}(t)=2a_n t+b_n \\ -g\le \ddot{y}(t)=2a_n \le ACC_{allowable}>0 \end{cases} \tag{A4}$$

Smoothness conditions (A5):

$$\begin{aligned} &a_n\alpha_n^{\,2}+b_n\alpha_n+c_n-m_n\alpha_n-h_n=0 \quad , \quad 2a_n\alpha_n+b_n-m_n=0 \quad , \\ &a_n\beta_n^{\,2}+b_n\beta_n+c_n-m_{n+1}\beta_n-h_{n+1}=0 \quad , \quad 2a_n\beta_n+b_n-m_{n+1}=0 \quad , \quad 2\le n\le N-1 \end{aligned} \tag{A5}$$

Either τ_n which is introduced in (A4) or the allowable acceleration that can be tolerated, ie $ACC_{allowable}^{Max}$ and that required for holding vehicle-road contact, ie $ACC_{allowable}^{Min}$, can be imposed to a problem. Consider for instance options of (A6).

$$either \quad \tau_n \equiv \frac{1}{10}\,Minimum\{t_{n+1}-t_n\,,\ t_n-t_{n-1}\}$$

$$or \quad \begin{cases} ACC_{allowable}^{Max}=g \\ ACC_{allowable}^{Min}=-g \end{cases} \Rightarrow \quad -g\le \ddot{y}(t)=2a_n=\frac{m_{n+1}-m_n}{\tau_n}\le g \Rightarrow -g\le \frac{m_{n+1}-m_n}{\tau_n}\le g$$
$$\Rightarrow \quad \tau_n \ge \frac{|m_{n+1}-m_n|}{g} \Rightarrow \tau_n=\frac{|m_{n+1}-m_n|}{g} \tag{A6}$$

Having τ_n from either options of (A6), the unknowns are found as given by (A7).

$$\begin{aligned} &a_n=\frac{m_{n+1}-m_n}{2\tau_n} \quad , \quad \alpha_n=\frac{-\tau_n}{2}-\frac{h_{n+1}-h_n}{m_{n+1}-m_n} \quad , \quad \beta_n=\alpha_n+\tau_n \quad , \quad b_n=m_n-2a_n\alpha_n \quad , \\ &c_n=h_n+(m_n-b_n)\alpha_n-a_n\alpha_n^{\,2} \quad , \quad 2\le n\le N-1 \end{aligned} \tag{A7}$$

Persian Abstract

چکیده

نیروی وارد بر چرخ خودرو در مدل ۱/۲ که با سرعت ثابت حرکت می¬کند با در نظر گرفتن ناهمواری جاده، آیرودینامیک و شرایط آب و هوایی مانند دما و رطوبت هوا محاسبه شده است. یک جاده با ناهمواری کلاس D مطابق با استاندارد ISO-8606 برای انجام آزمایش انتخاب شد و پروفیل سطح آن با استفاده از یک دوربین توپوگرافی از سری Leica اندازه¬گیری شد تا داده¬های گسسته به منظور مدل¬سازی زبری جاده بدست آید. داده¬ها از حالت گسسته به پیوسته هموار با استفاده از توابع خطی درجه دوم تبدیل شدند، با توجه به این واقعیت که معادلات دیفرانسیل حرکت خودرو وابسته به ناهمواری جاده و نرخ زمان تغییرات آن است. چنین فرض شده است که خط اثر باد یا نیروی آیرودینامیکی اعمال شده به مدل خودرو از مرکز جرم خودرو می¬گذرد. برای بدست آوردن ارتعاشات مدل ۱/۲ خودرو از روش رانگ-کوتا استفاده شده است. از طراحی آزمایش به منظور بررسی اثرات دما و رطوبت هوا بر چرخ¬های عقب و جلو استفاده شده است. مشخص شد که نیروی وارد به چرخ جلوی خودرو به مراتب بیشتر از نیرویی است که به چرخ عقب خودرو وارد می¬شود (حدود ۱۶/۵ درصد). همچنین، اثر دمای هوا بر نیروی چرخ بسیار بیشتر از اثر رطوبت هوا است. علاوه بر این، نیروی چرخ جلو با مقادیر پارامترهای آب و هوایی رابطه مستقیم دارد و رابطه نیروی چرخ عقب با آنها بصورت عکس است.